PERGAMON

International Journal of Solids and Structures 38 (2001) 4879–4899

INTERNATIONAL JOURNAL OF SOLIDS and STRUCTURES

www.elsevier.com/locate/ijsolstr

Statistics of the elastic behaviour of granular materials

N.P. Kruyt [a,*], L. Rothenburg [b]

[a] *Department of Mechanical Engineering, University of Twente, P.O. Box 217, 7500 AE Enschede, Netherlands*
[b] *Department of Civil Engineering, University of Waterloo, Waterloo, Ont., Canada N2L 3G1*

Received 13 January 2000; in revised form 26 July 2000

Abstract

The elastic behaviour of isotropic assemblies of granular materials consisting of two-dimensional, bonded and non-rotating particles is studied from the micromechanical viewpoint. Discrete element simulations have been performed of assemblies of 50,000 particles with various coordination numbers (average number of contacts per particle) and various ratios of tangential to normal stiffness. Statistics, such as mean, standard deviation and probability distribution function, have been computed for geometrical quantities and contact displacements under compressive and shearing loading. A linear relation is observed between the average number of contacts of a particle and its circumference. Average displacements do not conform to (generalised) uniform strain as is often assumed. The probability density functions for normal and tangential displacements are nearly Gaussian. None of the considered energies satisfy an equipartition of energy between normal and tangential modes.

Keywords: Granular materials; Micromechanics; Elasticity

1. Introduction

A detailed knowledge of the mechanical behaviour of granular materials is of great importance in various geotechnical and industrial applications. This knowledge is expressed by a constitutive relation that is usually based on continuum mechanics. Often, phenomenological assumptions are made to obtain the constitutive relation.

Micromechanics is a completely different approach for modelling the mechanical behaviour of granular materials. In contrast to the continuum viewpoint, it fully recognises the heterogeneous and discrete nature of granular materials. In micromechanics, a granular material is modelled as an assembly of semi-rigid particles interacting by means of contact forces. The objective is to develop macroscopic (continuum) constitutive relations from the microscopic (contact) constitutive relations, using suitable averaging techniques. Some recent micromechanical studies are Rothenburg (1980), Christoffersen et al. (1981), Digby (1981), Walton (1987), Bathurst and Rothenburg (1988a,b), Cundall et al. (1989), Chang et al. (1990, 1999), Rothenburg and Bathurst (1991, 1992), Bagi (1993, 1995), Chang and Liao (1994), Cambou et al. (1995),

* Corresponding author. Tel.: +31-53-489-2528; fax: +31-53-489-3695.
E-mail address: n.p.kruyt@wb.utwente.nl (N.P. Kruyt).

0020-7683/01/$ - see front matter
PII: S0020-7683(00)00313-9

Ostoja-Starzewski et al. (1995), Kruyt and Rothenburg (1996, 1998) and Alzebdeh and Ostoja-Starzewski (1999).

Here, a detailed micromechanical study is carried out on the elastic behaviour of isotropic assemblies of two-dimensional, bonded and *non-rotating* particles. The results of this study suggest directions for further theoretical developments.

The case of two-dimensional, bonded and *non-rotating* disks is considered here since it constitutes a simple model. It is expected that many salient features of this system will hold (qualitatively) for more complicated systems. Some applications of the current model are the initial elastic deformation of dense or cemented granular materials and certain fibrous media.

Since the packing of real granular materials is heterogeneous, the mechanical response will also be heterogeneous and exhibit random variations. This implies the usefulness of a statistical approach. To obtain the necessary data, discrete element simulations, as proposed by Cundall and Strack (1979), have been performed on assemblies consisting of 50,000 particles. Discrete element simulations were employed since they provide such detailed information at the microscopic level, which would be very hard (if possible at all) to obtain from (photoelastic) experiments (for example, de Josselin de Jong and Verruijt, 1969; Drescher and de Josselin de Jong, 1972; Oda and Konishi, 1974). In effect, the displacements and forces for all particles are computed. From the results of the simulations, statistics such as mean, standard deviation and probability distribution function were computed for various quantities of interest. The computed statistical quantities are expected to be reliable since such a large number of particles is used in the simulations. Some probability density functions for displacements for non-elastic behaviour are given by Cundall et al. (1989), Bagi (1993) and Oger et al. (1998).

The outline of this paper is as follows: First, an overview of micromechanics of granular materials is given. This is followed by a description of the discrete element simulation technique, the employed assemblies and the averaging procedures for obtaining various statistics. Then, the results are presented for the elastic moduli, geometry, displacements and various energies. Finally, the results of this study are discussed.

2. Micromechanics

Micromechanics of granular materials deals with the study of microscopic properties of particles, and their relation with overall characteristics. For granular materials, particles only exert forces on one another when they are in contact. For the quasi-static deformations considered here, the objective of micromechanics is to find the macroscopic characteristics (overall stress $\boldsymbol{\sigma}$ and strain $\boldsymbol{\varepsilon}$) from the characteristics at the microscopic level (contacts). The relevant physical quantities at the contacts are contact force $\boldsymbol{f}^c$ and contact relative displacement $\boldsymbol{\Delta}^c$. The macroscopic constitutive relation relates the average macroscopic stress tensor $\boldsymbol{\sigma}$ to the average macroscopic strain tensor $\boldsymbol{\varepsilon}$, whereas the microscopic contact constitutive relation relates force $\boldsymbol{f}^c$ to relative displacement between particle centres $\boldsymbol{\Delta}^c$ at the contact point. The contact geometry is depicted in Fig. 1: $\boldsymbol{n}^c$ and $\boldsymbol{t}^c$ are the normal and tangential vector of the contact, respectively, and $\boldsymbol{X}^p$ is the centre of particle p. The displacement of the centre of particle p is denoted by $\boldsymbol{u}^p$. The orientation of a contact θ^c is defined by the direction of its normal vector $\boldsymbol{n}^c$. The contact relative displacement between particles q and p is defined by

$$\boldsymbol{\Delta}^{pq} = \boldsymbol{u}^q - \boldsymbol{u}^p. \tag{1}$$

Branch vectors $\boldsymbol{l}^c$ are defined as the vectors that connect the centres of particles that are in contact. These branch vectors form closed loops or networks that define polygons (Fig. 2). The vectors that connect the centres of adjacent polygons are the rotated polygon vectors $\boldsymbol{g}^c$. The rotated polygon vectors also form closed loops that are shown in Fig. 2. The *polygon vectors* $\boldsymbol{h}^c$ are obtained by rotating the rotated polygon

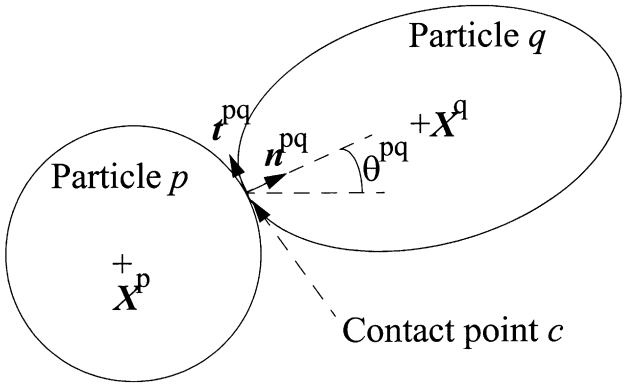

Fig. 1. Contact geometry.

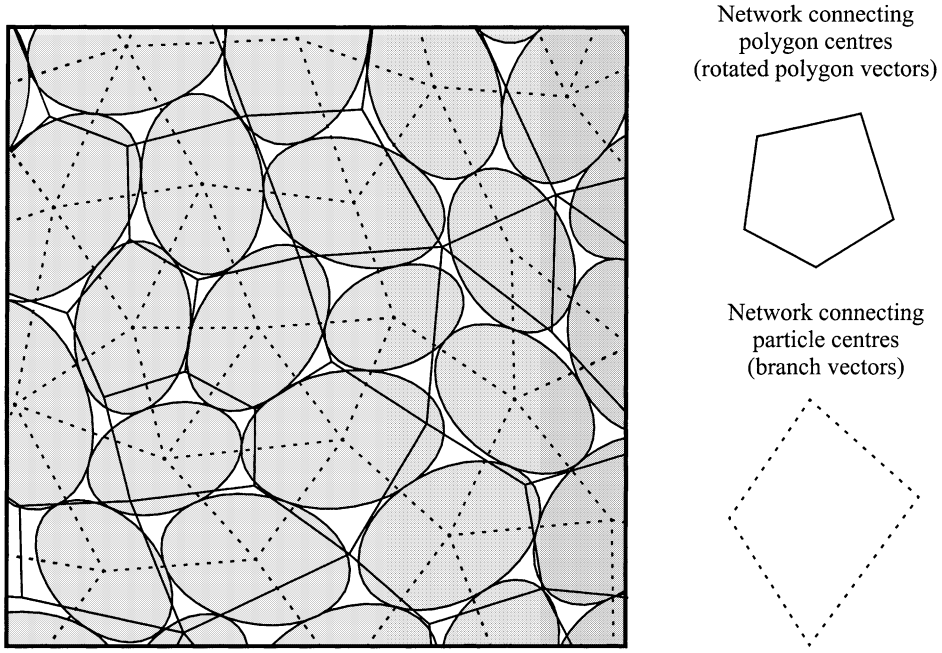

Fig. 2. Networks of branch and rotated polygon vectors.

vectors counterclockwise over 90°. The graph formed by the rotated polygon vectors is the dual (see for example Liu (1968)) of that formed by the branch vectors. Some properties of these graphs are discussed by Satake (1992).

The number of particles is N_p, N_c is the number of contacts and N_l is the number of polygons (loops). Euler's relation for planar graphs is, see for example Liu (1968): $N_p - N_c + N_l = 1$. For large assemblies, the right-hand side is negligible:

$$N_p - N_c + N_l \cong 0. \tag{2}$$

Denoting the average number of contacts per particle or the *average coordination number* by Γ and the average number of sides per polygon by Ω, it follows from Eq. (2) after noting that each contact is "shared" by two particles and two polygons,

$$N_c = \frac{\Gamma}{2} N_p, \qquad N_c = \frac{\Omega}{2} N_l, \qquad \Omega \cong \frac{2\Gamma}{\Gamma - 2}. \tag{3}$$

The quasi-static equilibrium conditions for particle p are

$$\boldsymbol{f}^{p\beta} + \sum_q \boldsymbol{f}^{pq} = \mathbf{0}, \tag{4}$$

where $\boldsymbol{f}^{p\beta}$ is the force exerted by the boundary on particle p and the summation is over the particles q that are in contact with particle p.

The compatibility conditions for the relative displacements of particle centres are

$$\boldsymbol{\Delta}^{r\alpha} + \sum_s \boldsymbol{\Delta}^{rs} = \mathbf{0}, \tag{5}$$

where $\Delta^{r\alpha}$ is the relative displacement between the boundary and contact r and the summation is over the sides (contacts) s that form polygon r.

Since the branch and polygon vectors form closed loops, they satisfy

$$\sum_s \boldsymbol{l}^{rs} = \mathbf{0}, \tag{6}$$

$$\sum_q \boldsymbol{h}^{pq} = \mathbf{0}. \tag{7}$$

In terms of contact quantities, the macroscopic stress tensor (for example, Drescher and de Josselin de Jong, 1972; Strack and Cundall, 1978; Rothenburg and Selvadurai, 1981) and strain tensor (Kruyt and Rothenburg, 1996) are expressed by

$$\boldsymbol{\sigma} = \frac{1}{S} \sum_{c \in S} \boldsymbol{f}^c \boldsymbol{l}^c, \tag{8}$$

$$\boldsymbol{\varepsilon} = \frac{1}{S} \sum_{c \in S} \boldsymbol{\Delta}^c \boldsymbol{h}^c, \tag{9}$$

where the sum is over all contacts c in the region of interest with area S. Note that this expression for the strain tensor involves the relative displacement at the contact, whereas the expression of Strack and Cundall (1978) contains the absolute displacements. It is the relative displacement at the contact that is linked through the contact constitutive relation to the contact forces. The expression of Strack and Cundall (1978) is therefore of limited use in micromechanical studies.

A geometrical relation between branch and polygon vectors is (Kruyt and Rothenburg, 1996)

$$\mathbf{I} = \frac{1}{S} \sum_{c \in S} \boldsymbol{l}^c \boldsymbol{h}^c, \tag{10}$$

where $\mathbf{I}$ is the identity tensor. This equation states that the tessellation of polygons covers the entire area S.

The work done at the boundaries must equal the work done at the contacts (Kruyt and Rothenburg, 1998). Hence,

$$\boldsymbol{\sigma} : \boldsymbol{\varepsilon} = \frac{1}{S} \sum_{c \in S} \boldsymbol{f}^c \cdot \boldsymbol{\Delta}^c. \tag{11}$$

2.1. Group averaging

For large assemblies that are random and spatially homogeneous, discrete quantities like those in Eqs. (8) and (9) can be replaced by continuous distributions by grouping contacts with similar orientation θ. An example of this *group averaging* is the contact distribution function $E(\theta)$ (Horne, 1965): $E(\theta)\Delta\theta$ is the fraction of contacts with orientation within the interval $(\theta, \theta + \Delta\theta)$. For the isotropic assemblies considered here $E(\theta) = 1/(2\pi)$.

For an arbitrary contact quantity α, its group average is denoted by $\bar{\alpha}(\theta)$, while an overall average over all orientations $\langle\bar{\alpha}\rangle$ is defined by

$$\langle\bar{\alpha}\rangle = m_S \int_{-\pi}^{\pi} \bar{\alpha}(\theta) E(\theta)\, \mathrm{d}\theta, \tag{12}$$

where m_S is the contact density with respect to area $m_S = N_c/S$.

Since a contact can be "viewed" from two particles, contacts with orientation θ and $-\theta$ are equivalent. Therefore, the contact distribution function E and the normal and tangential components of the contact force f_n and f_t satisfy

$$E(-\theta) = E(\theta), \qquad \overline{f}_\mathrm{n}(-\theta) = \overline{f}_\mathrm{n}(\theta), \qquad \overline{f}_\mathrm{t}(-\theta) = \overline{f}_\mathrm{t}(\theta). \tag{13}$$

Of course, similar relations hold for the branch, polygon and relative displacement vectors. It therefore suffices to consider only orientations θ in the interval $(0°, 180°)$.

In terms of group averages, the stress tensor (8) and strain tensor (9) are given by

$$\sigma = \langle\overline{\boldsymbol{f}\boldsymbol{l}}\rangle, \qquad \boldsymbol{\varepsilon} = \langle\overline{\boldsymbol{\Delta}\boldsymbol{h}}\rangle. \tag{14}$$

2.2. Contact constitutive relation

In the micromechanical approach, the mechanical behaviour of the materials is specified at the microscopic (contact) level. Attention is focused here on the (linear) elastic behaviour of bonded assemblies. Here, only the case of two-dimensional assemblies of *non-rotating* particles is considered. The linear contact constitutive relation relates the normal and tangential forces, f_n^c and f_t^c, at the contact to the normal and tangential components, Δ_n^c and Δ_t^c, of the relative displacement of the two particles involved and to the stiffnesses, k_n and k_t, of springs in normal and tangential direction

$$f_\mathrm{n}^c = k_\mathrm{n} \Delta_\mathrm{n}^c \qquad f_\mathrm{t}^c = k_\mathrm{t} \Delta_\mathrm{t}^c. \tag{15}$$

The ratio between tangential and normal stiffness is denoted by the stiffness ratio $\lambda = k_\mathrm{t}/k_\mathrm{n}$.

The relation between force and relative displacement at the contact is expressed by the stiffness matrix $\boldsymbol{S}^c$

$$\boldsymbol{f}^c = \boldsymbol{S}^c \cdot \boldsymbol{\Delta}^c, \qquad \boldsymbol{S}^c = k_\mathrm{n} \boldsymbol{n}^c \boldsymbol{n}^c + k_\mathrm{t} \boldsymbol{t}^c \boldsymbol{t}^c. \tag{16}$$

With this linear elastic contact constitutive relation, the macroscopic (continuum) constitutive relation is also elastic. The strain tensor $\boldsymbol{\varepsilon}$ is related to the stress tensor $\boldsymbol{\sigma}$ by the effective elastic stiffness tensor $\mathbf{L}$ and compliance tensor $\mathbf{M}$

$$\boldsymbol{\sigma} = \boldsymbol{L} : \boldsymbol{\varepsilon}, \qquad \boldsymbol{\varepsilon} = \boldsymbol{M} : \boldsymbol{\sigma}. \tag{17}$$

An overview of the micromechanical relations is given in Table 1.

Table 1
Overview of micromechanical relations

Particle	Connecting relation	Polygon
$\sum_q \boldsymbol{h}^{pq} = 0$	$\mathbf{I} = \frac{1}{S}\sum_{c\in S} \boldsymbol{h}^c \boldsymbol{l}^c$	$\sum_s \boldsymbol{l}^{rs} = \mathbf{0}$
$\sum_q \boldsymbol{f}^{pq} = \mathbf{0}$	$\boldsymbol{f}^c = \boldsymbol{S}^c \cdot \boldsymbol{\Delta}^c$	$\sum_s \boldsymbol{\Delta}^{rs} = \mathbf{0}$
$\boldsymbol{\sigma} = \frac{1}{S}\sum_{c\in S} \boldsymbol{f}^c \boldsymbol{l}^c$	$\boldsymbol{\sigma} : \boldsymbol{\varepsilon} = \frac{1}{S}\sum_{c\in S} \boldsymbol{f}^c \cdot \boldsymbol{\Delta}^c$	$\boldsymbol{\varepsilon} = \frac{1}{S}\sum_{c\in S} \boldsymbol{\Delta}^c \boldsymbol{h}^c$

2.3. Uniform strain and uniform stress

With the linear contact constitutive relation, upper and lower bounds on the stiffness tensor were derived by Kruyt and Rothenburg (1998) from minimum potential and minimum complementary energy principles. The upper bound corresponds to uniform strain, while the lower bound corresponds to uniform stress. These two regimes are characterised by

$$\begin{aligned} &\text{uniform strain}: \quad \boldsymbol{\Delta}^c = \boldsymbol{\varepsilon} \cdot \boldsymbol{l}^c, \\ &\text{uniform stress}: \quad \boldsymbol{f}^c = \boldsymbol{\sigma} \cdot \boldsymbol{h}^c. \end{aligned} \tag{18}$$

Note that the relative displacement field according to uniform strain satisfies the compatibility conditions for *all* loops (see Eqs. (6), (9) and (10)), while the force field according to uniform stress satisfies the equilibrium conditions for *all* particles (see Eqs. (7), (8) and (10)).

The stiffness tensor according to uniform strain $\boldsymbol{L}^{\varepsilon}$ and the compliance tensor according to uniform stress $\boldsymbol{M}^{\sigma}$ are given by Kruyt and Rothenburg (1996, 1998)

$$L^{\varepsilon}_{ijkl} = \langle S_{ik}\overline{l_j l_l}\rangle, \qquad M^{\sigma}_{ijkl} = \langle S^{-1}_{ik}\overline{h_j h_l}\rangle. \tag{19}$$

These expressions involve group averages of branch and polygon vectors. For isotropic assemblies, we have

$$\begin{aligned} &\overline{\boldsymbol{l}}(\theta) = \overline{l_{\mathrm{n}}}\boldsymbol{n}(\theta), \qquad \overline{\boldsymbol{ll}}(\theta) = \overline{l^2_{\mathrm{n}}}\boldsymbol{n}(\theta)\boldsymbol{n}(\theta) + \overline{l^2_{\mathrm{t}}}\boldsymbol{t}(\theta)\boldsymbol{t}(\theta), \\ &\overline{\boldsymbol{h}}(\theta) = \overline{h_{\mathrm{n}}}\boldsymbol{n}(\theta), \qquad \overline{\boldsymbol{hh}}(\theta) = \overline{h^2_{\mathrm{n}}}\boldsymbol{n}(\theta)\boldsymbol{n}(\theta) + \overline{h^2_{\mathrm{t}}}\boldsymbol{t}(\theta)\boldsymbol{t}(\theta), \end{aligned} \tag{20}$$

where $\overline{l_{\mathrm{n}}}$, $\overline{h_{\mathrm{n}}}$, $\overline{l^2_{\mathrm{n}}}$, $\overline{l^2_{\mathrm{t}}}$, $\overline{h^2_{\mathrm{n}}}$ and $\overline{h^2_{\mathrm{t}}}$ are independent of orientation θ.

The corresponding uniform field moduli are

$$\begin{aligned} &\frac{K^{\varepsilon}}{k_{\mathrm{n}}} = \frac{m_S}{4}(\overline{l^2_{\mathrm{n}}} + \lambda\overline{l^2_{\mathrm{t}}}), \qquad \frac{G^{\varepsilon}}{k_{\mathrm{n}}} = \frac{m_S}{8}(1+\lambda)(\overline{l^2_{\mathrm{n}}} + \overline{l^2_{\mathrm{t}}}), \\ &\frac{K^{\sigma}}{k_{\mathrm{n}}} = \frac{\lambda}{m_S(\lambda\overline{h^2_{\mathrm{n}}} + \overline{h^2_{\mathrm{t}}})}, \qquad \frac{G^{\sigma}}{k_{\mathrm{n}}} = \frac{2\lambda}{m_S(1+\lambda)(\overline{h^2_{\mathrm{n}}} + \overline{h^2_{\mathrm{t}}})}, \end{aligned} \tag{21}$$

where K^{ε} and K^{σ} are bulk moduli and G^{ε} and G^{σ} are shear moduli.

Expressions for K^{ε} and G^{ε} were already given by Bathurst and Rothenburg (1988a) for disks. Note that for disks, as will be considered in the sequel,

$$l_{\mathrm{t}} \equiv 0. \tag{22}$$

3. Discrete element simulations

Discrete element simulations, as proposed by Cundall and Strack (1979), are computer simulations in which the motion of a large assembly of particles (the discrete elements) is computed. The movement of the particles, induced by stress or strain at the boundary, is computed from the equations of motion.

There are three main aspects to discrete element simulations

- particle shape and particle size distribution,
- contact constitutive relation,
- numerical method for solving equations of motion.

The numerical method employed here for quasi-static motion is the time-stepping method of Cundall and Strack (1979) with underrelaxation instead of damping.

3.1. Particle size distribution

Various particle shapes have been employed: (i) disks, as originally used by Cundall and Strack (1979) and also used here, (ii) ellipses (Rothenburg and Bathurst, 1991; Ting, 1992), or (iii) polygons (Cundall, 1988).

The geometry of the particles is completed by specifying the particle size distribution. The selected particle size distribution for the particle radius R is a lognormal distribution that is frequently used for granular materials (see for example Prasher, 1987). Its probability density function P is given by

$$P(R;R_{\mathrm{med}},\tau)=\frac{1}{\sqrt{2\pi\ln(1+\tau^2)}}\exp\left(-\frac{1}{2}\frac{[\ln(R)-\ln(R_{\mathrm{med}})]^2}{\ln(1+\tau^2)}\right), \tag{23}$$

where R_{med} is the median (i.e. the value where the cumulative probability function equals 1/2, (Fig. 3) and τ is ratio between standard deviation StdDev(R) and mean R_{avg}

$$R_{\mathrm{avg}}=R_{\mathrm{med}}\sqrt{1+\tau^2},\qquad \mathrm{StdDev}(R)=\tau R_{\mathrm{avg}}. \tag{24}$$

The employed particle size distribution is fairly wide with $\tau=0.25$. The corresponding probability density and cumulative probability functions are shown in Fig. 3. Note that the mean radius R_{avg} only determines the size of the area under consideration.

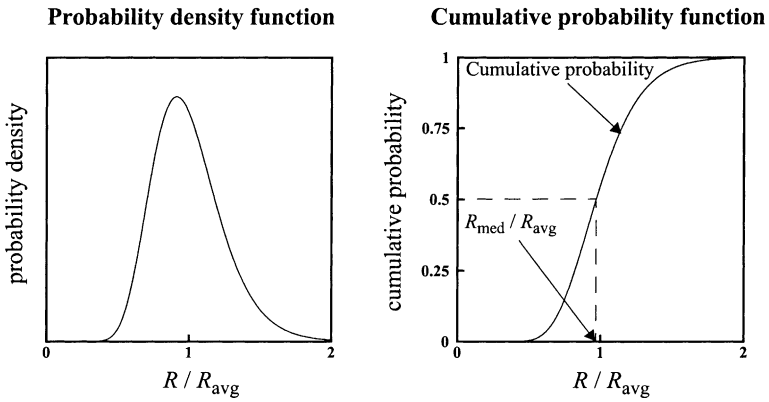

Fig. 3. Probability density and cumulative probability function of the lognormal distribution.

Particles were divided into 100 groups. The radii of the groups were selected in such a manner that the resulting cumulative probability function closely matched the lognormal cumulative probability function. The ratio between the radius of the largest disk in the simulations to that of the smallest is 3.7.

3.2. Assemblies

The assemblies of 50,000 disks that were used for the discrete element simulations were created by slow uniform compression until the required average coordination numbers Γ were obtained. Note that this compression was done in the "loose" mode where contacts were formed and lost, and hence significant particle rearrangement occurred. The assemblies generated in this manner were isotropic, as will be shown later (Fig. 6). Note that the average coordination number is a measure of the density of the packing. An approximate relation between solid fraction η and average coordination number Γ was derived by Kruyt and Rothenburg (1996), $\eta \cong (\pi/\Gamma)/\tan(\pi/\Gamma)$.

At higher average coordination numbers Γ, there may be a significant deformation, or "overlap", of the particles. Then, $R_1^c + R_2^c > l^c$, where R_1^c and R_2^c are the radii of the particles in contact c and l^c is the length of the branch vector. Since at the start of the elastic deformation all displacements and forces were reset to zero, the only effect of this "overlap" on the simulations is that it may obscure the relation between particle size distribution and the probability density function of the branch vector at higher average coordination numbers Γ.

3.3. Simulations

Discrete element simulations were performed for nine different isotropic assemblies with average coordination numbers Γ in the range 4–6, and for each average coordination number for nine different stiffness ratios λ in the range 0.05–1.0. Periodic boundaries (Cundall, 1986) were employed to minimize the disturbing influence of boundaries.

The assemblies were subjected to two strain paths in order to compute bulk modulus K and shear moduli G from

$$\begin{aligned} \sigma_{11} + \sigma_{22} &= 2K(\varepsilon_{11} + \varepsilon_{22}), \\ \sigma_{11} - \sigma_{22} &= 2G(\varepsilon_{11} - \varepsilon_{22}). \end{aligned} \tag{25}$$

The strain paths are

$$\begin{aligned} \text{compression}: \quad \boldsymbol{\varepsilon} &= \varepsilon \begin{bmatrix} -1 & 0 \\ 0 & -1 \end{bmatrix}, \\ \text{shear}: \quad \boldsymbol{\varepsilon} &= \varepsilon \begin{bmatrix} -1 & 0 \\ 0 & -1 \end{bmatrix}. \end{aligned} \tag{26}$$

The loading rate in the simulations was low enough that dynamic effects were negligible. This was verified by checking the linearity of the response and by performing simulations with a lower loading rate.

3.4. Averaging

Orientation-dependent quantities like the contact distribution function $E(\theta)$ were computed by dividing the range of orientations (0°, 180°) into 180 bins and computing the group averages for these bins. Probability density functions were computed by binning the relevant data into 100 bins.

4. Moduli

The overall bulk and shear moduli are shown in Fig. 4 for the average coordination numbers Γ and stiffness ratios λ that are considered. In all cases, the results for the moduli were bracketed by the upper (uniform strain) and lower (uniform stress) bounds that were derived by Kruyt and Rothenburg (1998).

The relation between upper and lower bounds and actual moduli is depicted in detail in Fig. 5 which shows that for average coordination number $\Gamma = 4$, the moduli lie in between the bounds, while for $\Gamma = 6$, the moduli follow the upper bound.

A comparison of the bulk and shear moduli for the cases with and without particle rotation is given by Kruyt and Rothenburg (1998). Results on the elastic properties obtained from simulations of three-dimensional assemblies are given by Chantawarangul (1993).

5. Geometry

In this section, properties of the geometry of the assemblies are studied. First, the isotropy of the contact distribution function $E(\theta)$ is checked. Then, the variation with average coordination number Γ of averages and standard deviations of branch and polygon vectors are shown. Finally, the probability density functions of branch and polygon vectors are given.

5.1. Contact distribution function

The contact distribution function is isotropic for all average coordination numbers Γ. Examples are shown in Fig. 6 for $\Gamma = 4$ and $\Gamma = 6$. The tangential component of the polygon vector is very small. Since the normal components of branch and polygon vector were even more direction-independent and smoother than the contact distribution function, these are not shown.

5.2. Averages and standard deviations

The variation of normal components of branch and polygon vectors with average coordination number Γ as well as the averages of squares (second moment) are shown in Fig. 7. The averages of squares of

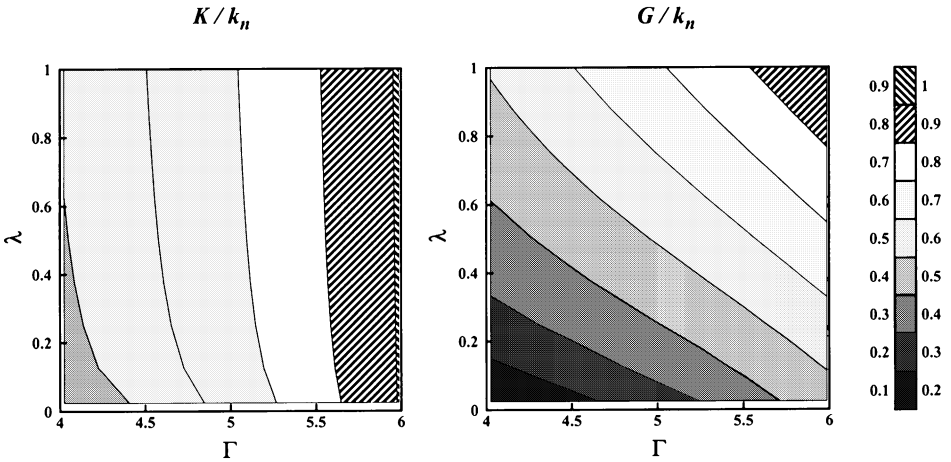

Fig. 4. Bulk and shear moduli from simulations.

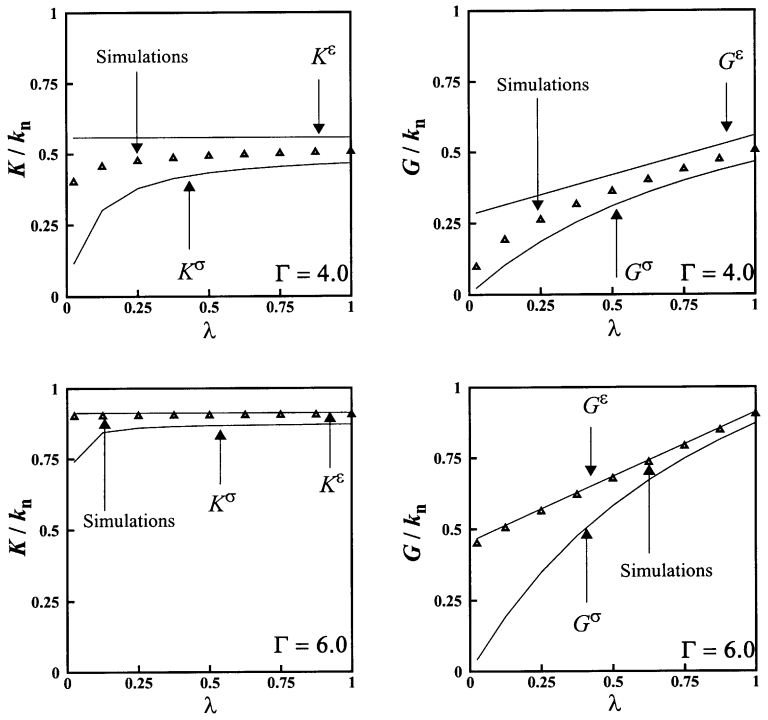

Fig. 5. Comparison between upper and lower bounds with actual bulk and shear modules.

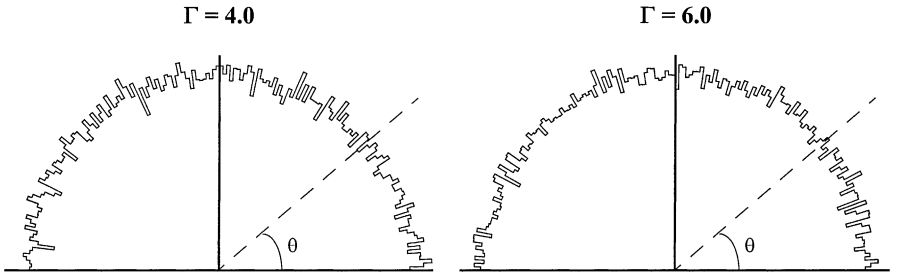

Fig. 6. Polar plots of contact distribution function $E(\theta)$ for average coordination number $\Gamma = 4$ and for $\Gamma = 6$; θ in (0°, 180°).

geometrical vectors are shown instead of standard deviations, since the squares are related to the bulk and shear moduli according to uniform strain and stress, (Eq. (21)). The standard deviation for l_n is fairly constant with Γ, while the standard deviation of h_n decreases rapidly with increasing Γ, and becomes very small at $\Gamma = 6$.

A qualitative explanation for the decrease in standard deviation of the polygon vector is that as $\Gamma \to 6$, the polygons form triangles ($\Omega \to 3$, see Eq. (3)). Since the polygons then consist of three branch vectors with fairly small standard deviation of their lengths, the standard deviation in the position of the centre of polygons (and hence in the polygon vectors) becomes even smaller.

A remarkable observation from Fig. 7 is that at average coordination number $\Gamma = 4$, the average branch vector $\overline{l}_n$ is *larger* (by 2.8%) than the average particle diameter $2R_{avg}$, while one would expect it to be *smaller* due to the "overlap" between particles. That for higher Γ, $\overline{l}_n$ no longer is larger than $2R_{avg}$ is not surprising,

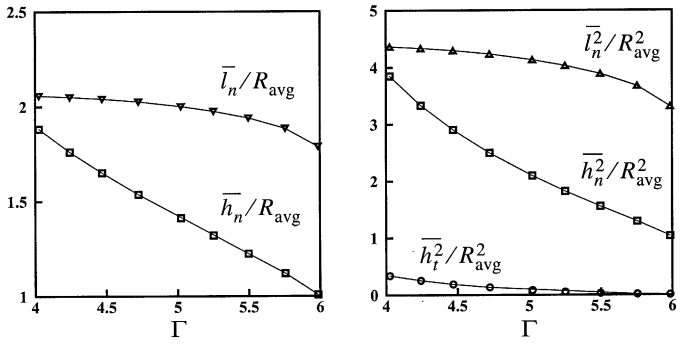

Fig. 7. Variation of mean and second moment of normal component of the branch and polygon vectors and tangential component of the polygon vector with average coordination number Γ.

since at higher Γ the "overlap" between particles leads to a reduction in $\overline{l}_n$. In micromechanical studies, the assumption is $\overline{l}_n = 2R_{avg}$ regularly made; see for example Walton (1987) and Cambou et al. (1995). The relation between average branch vector and average particle radius is analysed in detail in Section 5.3.

Simplified relations for some geometrical quantities were derived by Kruyt and Rothenburg (1996). These relations are

$$\frac{\overline{h}_n}{\overline{l}_n} \cong \tan\frac{\pi}{\Gamma}, \qquad m_S = \frac{2}{\overline{l}_n h_n} \cong \frac{2}{\overline{l}_n \overline{h}_n}. \tag{27}$$

These approximate relations are compared with the results from the simulations in Fig. 8. The agreement is good. Therefore, when more detailed information is missing, these approximate relations can be used.

5.3. Relation between radius and coordination number

The explanation for $\overline{l}_n > 2R_{avg}$ was found by investigating the relation between particle radius R and coordination number $\gamma(R)$ (Fig. 9). Apparently, there is a linear relation between the radius of a particle and its average number of contacts. A geometrical explanation is that the larger the circumference of a particle, the more contacts are formed. To investigate whether large particles tend to form contacts with other large

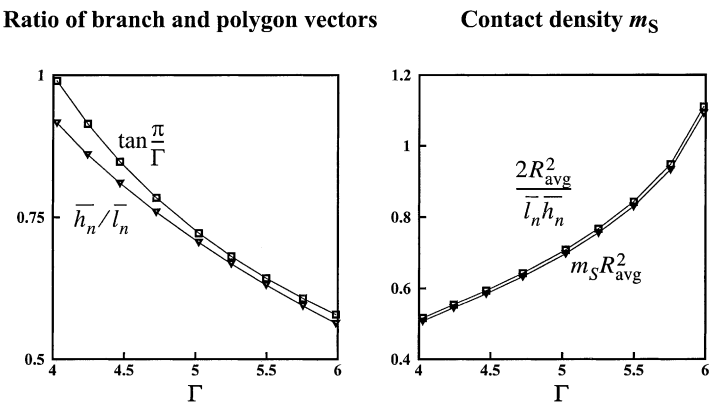

Fig. 8. Comparison of approximate and exact geometrical relations for the ratio of branch and polygon vectors and for contact density m_S.

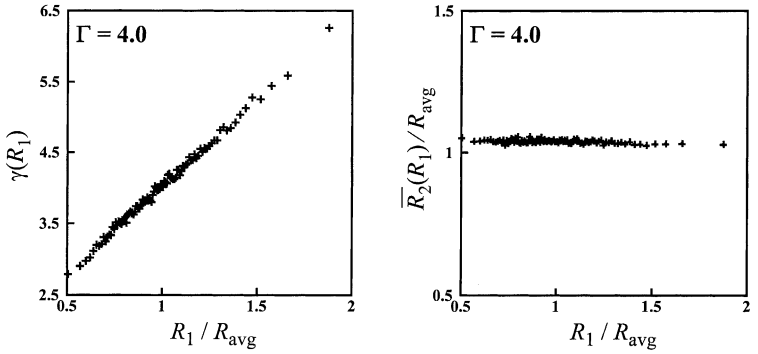

Fig. 9. Relation between particle radius and radius-dependent coordination number, and relation between radii of particles in contact. Data for the case of average coordination number $\Gamma = 4$.

particles, the relation between the radii of the two particles involved in a contact was computed. For all particles with radius R_1, the average over all contacts of the radius of the second particle involved, $\overline{R}_2(R_1)$, is computed. The result is given in Fig. 9 which shows that the two radii are uncorrelated (correlation coefficient of -0.009). Of course, for consistency, $\overline{R}_2(R_1)$ equals the average branch vector $\overline{l}_n/2$.

The linear relation

$$\gamma(R;\Gamma) = i(\Gamma) + s(\Gamma)R \tag{28}$$

was also observed at the other average coordination numbers Γ. A simple consistency relation exists between intercept $i(\Gamma)$ and slope $s(\Gamma)$ since

$$\Gamma = \int_R \gamma(R;\Gamma)p(R)\,\mathrm{d}R = \int_R [i(\Gamma) + s(\Gamma)R]p(R)\,\mathrm{d}R = i(\Gamma) + s(\Gamma)R_{\mathrm{avg}}, \tag{29}$$

where $p(R)$ is the particle size distribution function.

From the simulations, it was found that the intercept is given approximately by $i(\Gamma) \cong (\Gamma - 1)/2$. No explanation has been found for this linear relation.

A detailed analysis of the relation between branch vector and the particle size distribution follows. Since $N_c = N_p\Gamma/2$, it follows that *for disks* the average branch vector $\overline{l}_n$ is given by

$$\overline{l}_n = \frac{1}{N_c}\sum_c (R_1^c + R_2^c) = \frac{1}{N_c}\sum_p n_c(p)R_p = \frac{N_p}{N_c}\sum_R \gamma(R)Rp(R) = \frac{2}{\Gamma}\int_R \gamma(R)Rp(R)\,\mathrm{d}R, \tag{30}$$

where R_1^c and R_2^c are the radii of the particles involved in the contact and $n_c(p)$ is the number of contacts of particle p. Note that it is assumed that the "overlap" is negligible. When the coordination number does not depend on radius ($\gamma(R) \equiv \Gamma$), we find $\overline{l}_n = 2R_{\mathrm{avg}}$.

By a similar argument, we find

$$\overline{l_n^2} = \frac{1}{N_c}\sum_c (R_1^c + R_2^c)^2 = \frac{1}{N_c}\sum_p n_c(p)R_p^2 + \frac{2}{N_c}\sum_c R_1^c R_2^c. \tag{31}$$

Since the average of the radius of the second particle in a contact R_2^c equals, $\overline{l}_n/2$ independently of the radius of the first particle R_1^c (Fig. 9), it follows with Eq. (30)

$$\overline{l_n^2} = \frac{1}{N_c}\sum_p n_c(p)R_p^2 + \frac{1}{2}\overline{l}_n^2 = \frac{N_p}{N_c}\sum_R \gamma(R)R^2p(R) + \frac{1}{2}\overline{l}_n^2 = \frac{2}{\Gamma}\int_R \gamma(R)R^2p(R)\,\mathrm{d}R + \frac{1}{2}\overline{l}_n^2. \tag{32}$$

Using Eq. (30) this can be rewritten as

$$\overline{l_{\mathrm{n}}^2} - \overline{l}_{\mathrm{n}}^2 = \frac{2}{\Gamma} \int_R \gamma(R)[R - \overline{l}_{\mathrm{n}}/2]^2 p(R)\,\mathrm{d}R. \tag{33}$$

This gives the standard deviation of the normal component of the branch vector. When the coordination number does not depend on radius ($\gamma(R) \equiv \Gamma$),we find $\overline{l_{\mathrm{n}}^2} - \overline{l}_{\mathrm{n}}^2 = 2\mathrm{StdDev}(R)$. Substituting Eqs. (28) and (29) into Eq. (30) gives

$$\overline{l}_{\mathrm{n}} = 2R_{\mathrm{avg}} + \frac{2}{\Gamma} s(\Gamma)\mathrm{StdDev}(R)^2. \tag{34}$$

Since $s(\Gamma) \geqslant 0$, we do find that $\overline{l}_{\mathrm{n}} \geqslant 2R_{\mathrm{avg}}$.

For $\Gamma = 4.0$, the theoretical $\overline{l}_{\mathrm{n}}$ is larger than the observed $\overline{l}_{\mathrm{n}}$ by 1.0%, while the "overlap" then is approximately 0.6%. This "overlap" has been neglected in the derivations.

The linear relation between coordination number and particle radius (28) has only been investigated for the lognormal particle size distribution employed here with a single set of parameters for mean and standard deviation. It is recommended to investigate this relation for other parameters and other particle size distributions, including other particle shapes such as ellipses.

5.4. Probability density functions

Since the assemblies are isotropic, all contacts can be considered to compute probability density functions for the normal component of the branch vector and the normal and tangential components of the polygon vector. The results are shown in Fig. 10.

The probability density functions for the normal components of the branch and polygon vector resemble lognormal distributions. An example of the corresponding lognormal distribution (with the same mean and standard deviation) is also shown in Fig. 10.

The probability density function for the tangential component of the polygon vector has a strange distribution. However, the tangential component of the polygon vector is not very important in the isotropic case, since its mean is zero and its standard deviation is small (Fig. 7).

6. Displacements

In this section, the statistics of relative displacements are given. First, the direction dependence of the relative displacements will be shown. This is followed by results on the variation with average coordination number Γ and stiffness ratio λ of the magnitude of the relative displacements. Then, the probability density functions for the normal and tangential components of the relative displacements are given.

6.1. Direction-dependent displacements

The direction-dependent averages for normal and tangential components of the relative displacements were computed for compression and shear. As expected, the average tangential displacements were very small in compression. Typical examples of the polar plots are shown in Fig. 11.

6.2. Generalised uniform strain

The direction-dependent averages of relative displacements can be expressed by a generalised uniform strain field (Rothenburg, 1980; Bathurst and Rothenburg, 1988a,b)

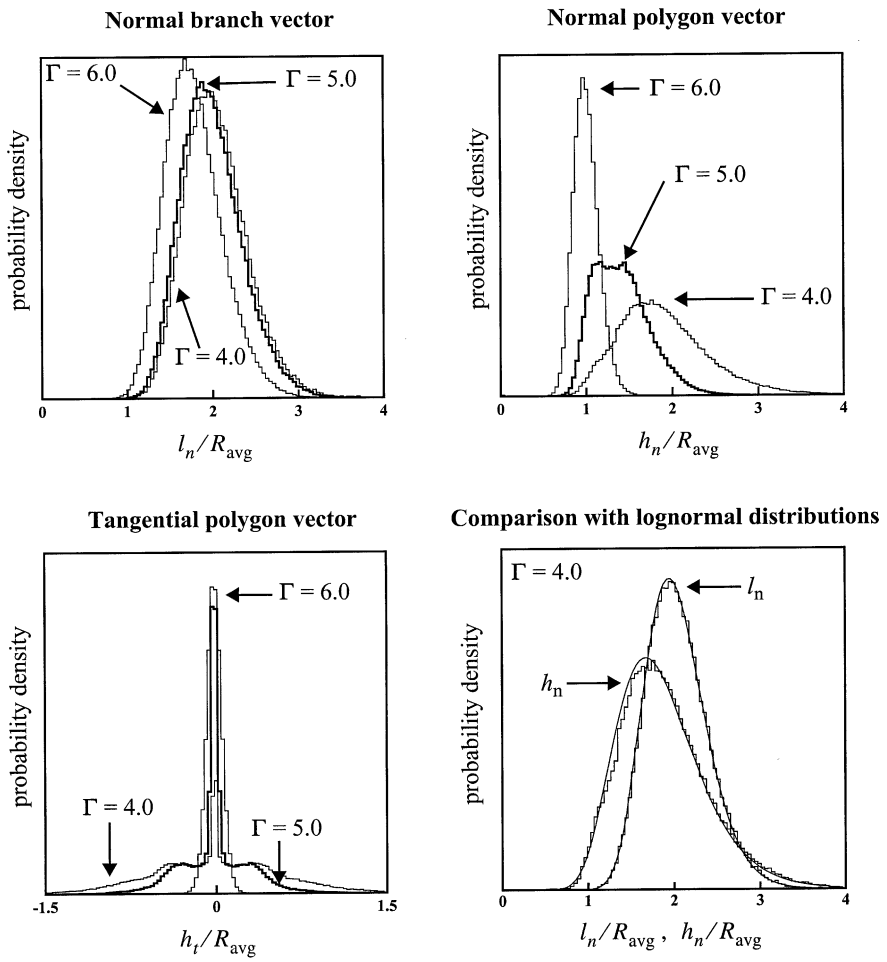

Fig. 10. Probability density function for the normal component of branch and polygon vectors and tangential component of polygon vector, and comparison with corresponding lognormal distributions for average coordination number $\Gamma = 4$.

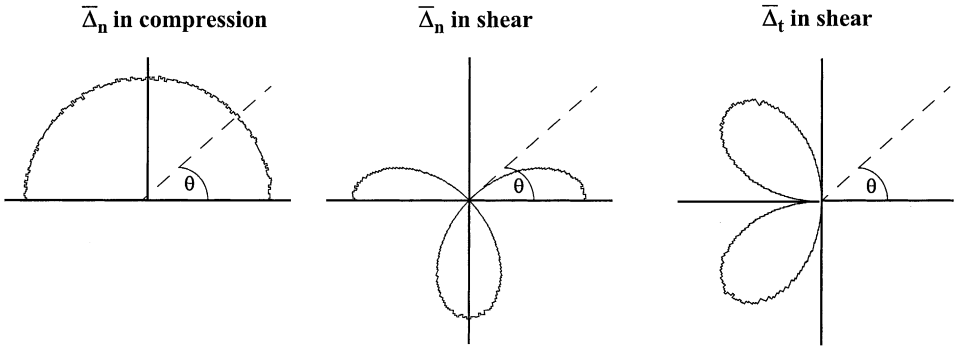

Fig. 11. Polar plot of orientation-dependent average of relative displacements for $\Gamma = 5$ and $\lambda = 0.5$; θ in (0°, 180°).

$$\overline{\Delta} = \zeta \boldsymbol{\epsilon} \cdot \bar{\boldsymbol{l}}. \tag{35}$$

Note that for uniform strain $\zeta = 1$.

With the strain paths according to Eq. (26), this gives for isotropic assemblies

$$\begin{aligned} &\text{compression}: \quad \overline{\Delta}_\mathrm{n} = \zeta_\mathrm{n}^K \varepsilon \bar{l}_\mathrm{n}, \quad \overline{\Delta}_\mathrm{t} = 0, \\ &\text{shear}: \quad \overline{\Delta}_\mathrm{n} = \zeta_\mathrm{n}^G \varepsilon \bar{l}_\mathrm{n} \cos 2\theta, \quad \overline{\Delta}_\mathrm{t} = -\zeta_\mathrm{t}^G \varepsilon \bar{l}_\mathrm{n} \sin 2\theta. \end{aligned} \tag{36}$$

In this manner, the direction-dependent averages of relative displacements are condensed into three numbers, two for normal (ζ_n^K for compression and ζ_n^G for shear) and one for tangential displacements (ζ_t^G for shear), that give the magnitude of the relative displacements. Note that the description (36) matches the direction-dependent averages of relative displacements that are shown in Fig. 11.

The factors ζ were computed from the simulations for all average coordination numbers Γ and all stiffness ratios λ. Different ζ are obtained for normal and tangential displacements and for different strain paths. The results are shown in Fig. 12.

From Fig. 12, it is clear that the (generalised) uniform strain assumption is incorrect. This assumption is often made in the literature, for example, Rothenburg (1980), Christoffersen et al. (1981), Digby (1981), Walton (1987), Bathurst and Rothenburg (1988a,b), Chang et al. (1990), Rothenburg and Bathurst (1991), Chang and Liao (1994), Cambou et al., (1995). Only at high average coordination number Γ, it is roughly correct. Remarkable is that $\zeta_\mathrm{t}^G > 1$, for which no explanation has been found yet.

Assuming that relative displacements and polygon vectors are *independent*, $\overline{\Delta \boldsymbol{h}} \cong \bar{\Delta} \bar{\boldsymbol{h}}$, as well as branch vectors and polygon vectors, $\overline{\boldsymbol{l}\boldsymbol{h}} \cong \bar{\boldsymbol{l}} \bar{\boldsymbol{h}}$, it follows from Eq. (36) that for consistency with the expression (14) for the strain tensor

$$\zeta_\mathrm{n}^K \cong 1, \qquad \tfrac{1}{2}[\zeta_\mathrm{n}^G + \zeta_\mathrm{t}^G] \cong 1. \tag{37}$$

Deviations of an order of magnitude of 15% from these expressions, Fig. 12, are primarily caused by the limited validity of the first assumption of independence (in particular $\overline{\Delta_\mathrm{t} h_\mathrm{t}} \neq \bar{\Delta}_\mathrm{t} \bar{h}_\mathrm{t}$ as $\overline{h}_\mathrm{t} = 0$), since the second assumption is justified by Fig. 8.

6.3. Probability density functions

The probability density functions for normal and tangential components of relative displacements were computed from the simulations for compression and shear. Since the distributions are direction-independent in compression, all contacts were used to compute the probability density function. In shear, this is not the case, and a range of orientation with a width of 10° was chosen where mean and standard deviation do not vary much. These ranges are different for normal and tangential displacements. Typical examples of the probability density functions are shown in Figs. 13 and 14, together with the corresponding Gaussian distribution. The probability density function for both normal and tangential distributions are nearly Gaussian, as was also found by Kruyt and Rothenburg (1998). In shear, the probability density functions are more "noisy" due to the smaller number of contacts used in their computation.

The (small) difference between the computed and the corresponding Gaussian distribution cannot be attributed to lack of accuracy due to insufficient data.

7. Energies

In this section, the orientation-dependent total and "scatter" energies are shown first. The "scatter" energies reflect the variances of relative displacement. Then, for all the considered average coordination

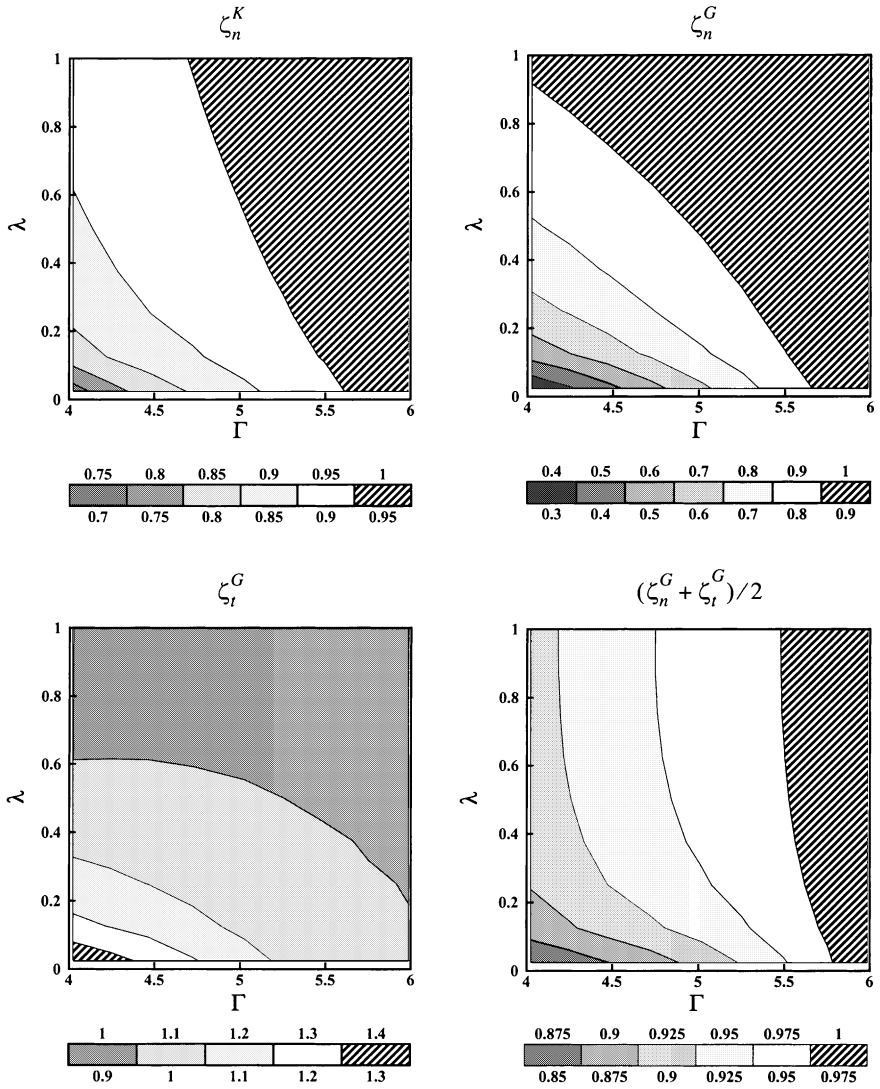

Fig. 12. Values of ζ from simulations.

numbers Γ and stiffness ratios λ, energy ratios are computed. These ratios are total energy in tangential mode over total energy in normal mode, and ratios of "scatter" energies over total energy.

7.1. Orientation-dependent energies

Orientation-dependent *total energy* in normal and tangential mode are defined by

$$\tfrac{1}{2}k_{\mathrm{n}}\overline{\Delta_{\mathrm{n}}^2}(\theta), \qquad \tfrac{1}{2}k_{\mathrm{t}}\overline{\Delta_{\mathrm{t}}^2}(\theta). \tag{38}$$

Orientation-dependent "scatter" *energy* in normal and tangential mode are defined by

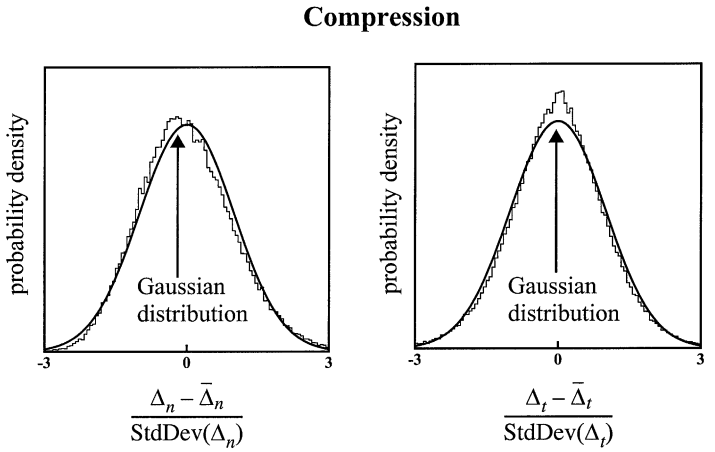

Fig. 13. Probability density functions for normal and tangential components of relative displacements together with the normalised Gaussian distribution in compression for average coordination number $\Gamma = 5$ and stiffness ratio $\lambda = 0.5$.

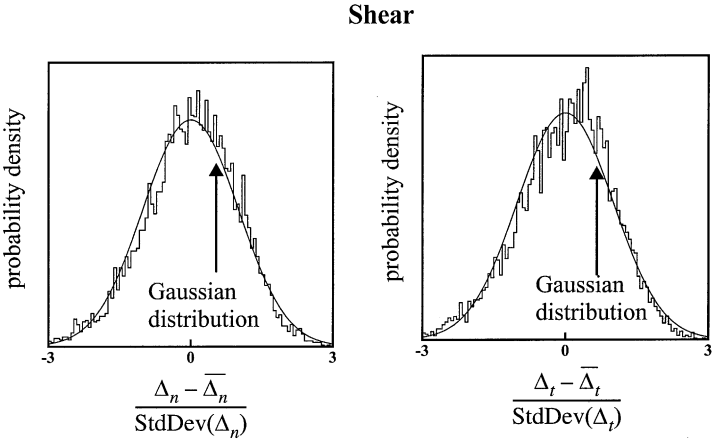

Fig. 14. Probability density functions for normal and tangential components of relative displacement together with the normalised Gaussian distribution in shear for average coordination number $\Gamma = 5$ and stiffness ratio $\lambda = 0.5$.

$$\tfrac{1}{2}k_{\mathrm{n}}\left[\overline{\Delta_{\mathrm{n}}^2}(\theta) - \overline{\Delta_{\mathrm{n}}}(\theta)^2\right], \qquad \frac{1}{2}k_{\mathrm{t}}\left[\overline{\Delta_{\mathrm{t}}^2}(\theta) - \overline{\Delta_{\mathrm{t}}}(\theta)^2\right]. \tag{39}$$

Polar plots of total energy in shear are shown Fig. 15, while those of "scatter" energy in shear are given in Fig. 16.

7.2. Energy ratios

Four different energies are defined here, the total energies E_{n} and E_{t} in normal and tangential modes, and the "scatter" energies Σ_{n} and Σ_{t} associated with deviations from the averages of normal and tangential components of relative displacements

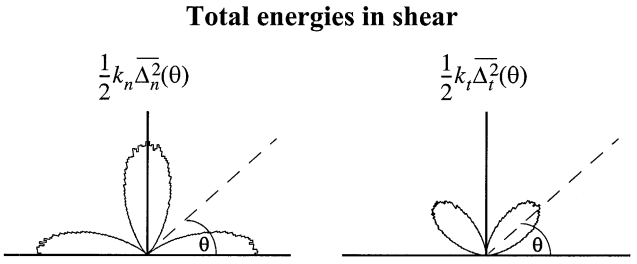

Fig. 15. Polar plot of orientation-dependent total energy in normal and tangential modes. Data for $\Gamma = 5$ and $\lambda = 0.5$ in shear; θ in (0°, 180°).

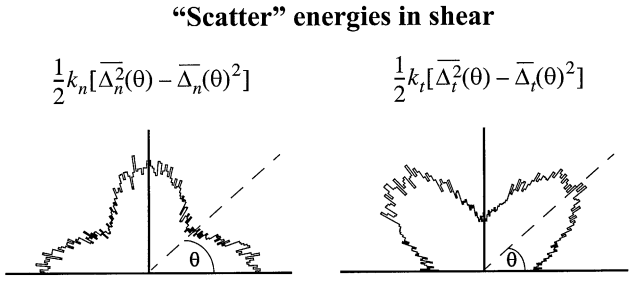

Fig. 16. Polar plots of orientation-depedent "scatter" in normal and tangential energies. Data for $\Gamma = 5$ and $\lambda = 0.5$ in shear; θ in (0°, 180°).

$$E_{\mathrm{n}} = \tfrac{1}{2}k_{\mathrm{n}}\langle\overline{\Delta_{\mathrm{n}}^2}(\theta)\rangle, \qquad E_{\mathrm{t}} = \tfrac{1}{2}k_{\mathrm{t}}\langle\overline{\Delta_{\mathrm{t}}^2}(\theta)\rangle,$$
$$\Sigma_{\mathrm{n}} = \tfrac{1}{2}k_{\mathrm{n}}\langle\overline{\Delta_{\mathrm{n}}^2}(\theta) - \overline{\Delta_{\mathrm{n}}}(\theta)^2\rangle, \qquad \Sigma_{\mathrm{t}} = \tfrac{1}{2}k_{\mathrm{t}}\langle\overline{\Delta_{\mathrm{t}}^2}(\theta) - \overline{\Delta_{\mathrm{t}}}(\theta)^2\rangle. \tag{40}$$

Statistical-mechanical studies of ideal gases, see for example Tolman (1938), lead to an equipartition of energy between the various modes. In analogy, the distribution between normal and tangential modes of the various energies has been computed here for all considered average coordination numbers Γ and stiffness ratios λ for compressive and shearing loading.

The ratio between the total energies in the tangential and normal modes is shown in Fig. 17 for compression and shear. It is clear that generally there is no equipartition between normal and tangential modes. Only in shear for high stiffness ratio λ, the energies approximately equal. Note the large contribution of the tangential mode at low average coordination number Γ and low stiffness ratio λ in shear. Essentially, no energy is present in the tangential mode in compression, as can be expected.

The ratio between "scatter" energy and total energy *in compression* is plotted in Fig. 18. The "scatter" energy in the tangential mode is low, while the "scatter" energy in the normal mode is of the order of magnitude of 10% for a wide range of average coordination numbers Γ and stiffness ratios λ.

The ratio between "scatter" energy and total energy *in shear* is plotted in Fig. 19. The "scatter" energy in the normal mode increases rapidly with decreasing stiffness ratio λ. The "scatter" energy in the tangential mode is smaller than that in the normal mode. It is less than 10% of the total energy for a wide range of average coordination numbers Γ and stiffness ratios λ.

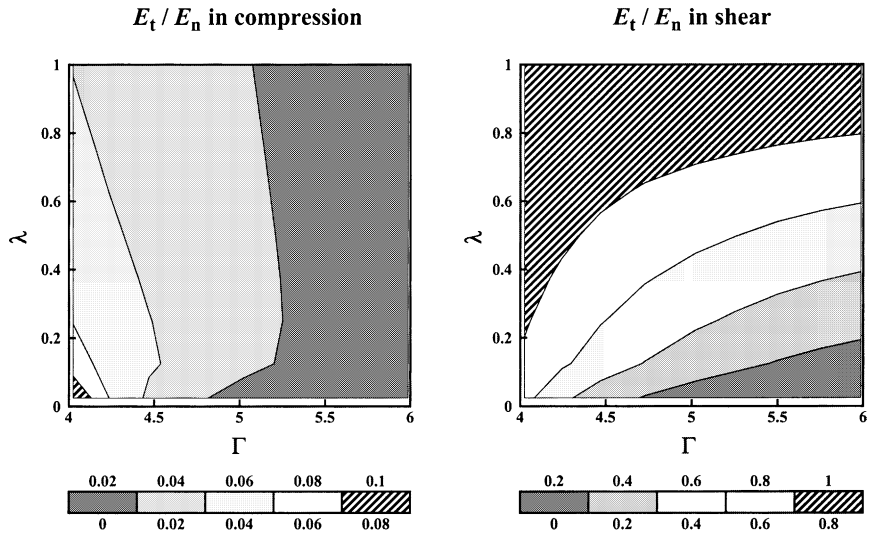

Fig. 17. Total energy ratio E_t/E_n in compression and in shear.

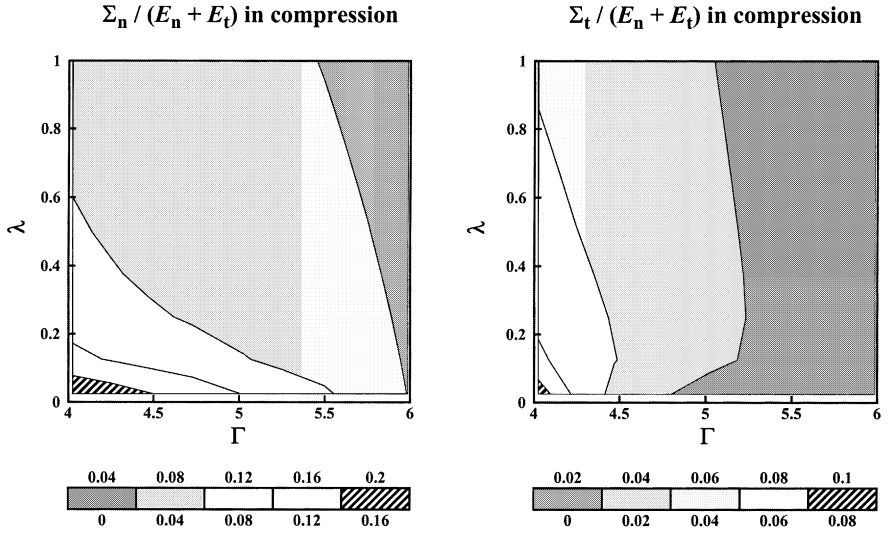

Fig. 18. Ratio between "scatter" energy and total energy for normal and tangential modes in compression.

8. Discussion

Based on discrete element simulations on large assemblies of 50,000 particles, a micromechanical study has been made on the statistics of various quantities. These quantities are geometry (branch and polygon vectors), displacements and various energies. The statistics that were considered were mean, standard deviation and probability density function.

The probability functions for the normal component of branch and polygon vectors resemble the particle size distribution; a lognormal distribution was used in the simulations. It was found that the coordination

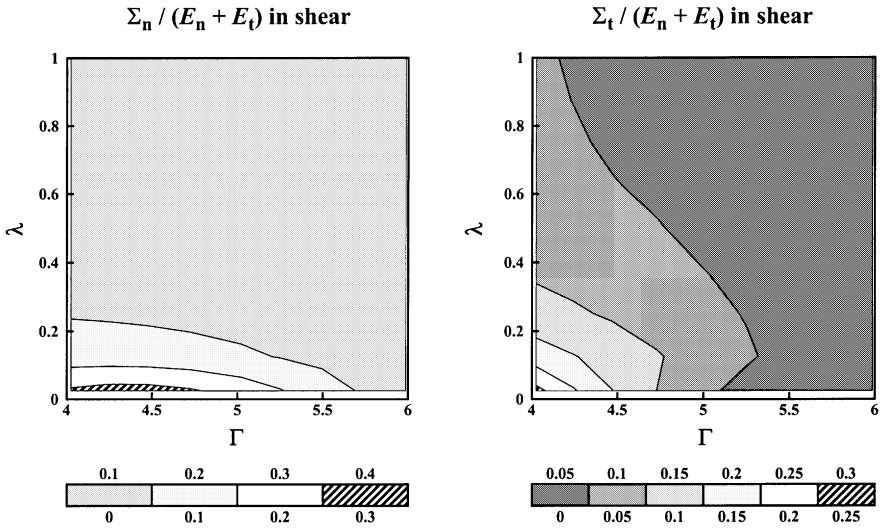

Fig. 19. Ratio between "scatter" energy and total energy for normal and tangential modes in shear.

number of particles depends on their radius. In fact, a linear relation between coordination number and radius was observed. This means that the probability of forming contacts increases linearly with the circumference of the particle.

The probability density functions for normal and tangential components of relative displacements closely match Gaussian distributions, although there are small deviations that cannot be attributed to lack of accuracy due to insufficient data.

The relative displacements do not correspond to uniform strain, as is frequently assumed in theories. In fact, a generalised continuum theory, see Eq. (35), is also not valid, since the calculated values for ζ are different for normal and tangential disagreements and they also depend on the strain path.

No equipartition of energy was found for the total and "scatter" energies that were considered. Only for the case of stiffness ratio $\lambda = 1.0$, there is equipartition of total energy. The "scatter" energies constitute a significant fraction of the total energy.

Finally, it is recommended to direct future research towards the more complicated cases of non-circular particle shapes (ellipses), two-dimensional assemblies *with* particle rotation and three-dimensional assemblies.

References

Alzebdeh, K., Ostoja-Starzewski, M., 1999. On a spring-network model and effective elastic moduli of granular materials. Journal of Applied Mechanics, Transactions of the ASME 66, 172–180.

Bagi, K., 1993. On the definition of stress and strain in granular assemblies through the relation between micro- and macro-level characteristics. Powders and Grains '93.

Bagi, K., 1995. Stress and strain in granular assemblies. Mechanics of Materials 22, 165–177.

Bathurst, R.J., Rothenburg, L., 1988a. Micromechanical aspects of isotropic granular assemblies with linear contact interactions. Journal of Applied Mechanics, Transactions of the ASME 55, 17–23.

Bathurst, R.J., Rothenburg, L., 1988b. Note on a random isotropic granular material with negative Poisson's ratio. International Journal of Engineering Science 26, 373–383.

Cambou, B., Dubujet, P., Emeriault, F., Sidoroff, F., 1995. Homogenisation for granular materials. European Journal of Mechanics A/Solids 14, 255–276.

Chang, C.S., Misra, A., Sundaram, S.S., 1990. Micromechanical modelling of cemented sands under low amplitude oscillations. Géotechnique 40, 251–263.

Chang, C.S., Liao, C.L., 1994. Estimates of elastic modulus for media of randomly packed granules. Applied Mechanics Review 47, S197–S206.

Chang, C.S., Shi, Q.S., Zhu, H., 1999. Microstructural modelling for elastic moduli of bonded granules. Journal of Engineering Mechanics, Transactions of the ASCE 125, 648–653.

Chantawarangul, K., 1993. Numerical simulations of three-dimensional granular assemblies. PhD Thesis, Department of Civil Engineering, University of Waterloo, Waterloo, Ontario, Canada.

Christoffersen, J., Mehrabadi, M.M., Nemat-Nasser, S., 1981. A micromechanical description of granular material behaviour. Journal of Applied Mechanics Transactions of the ASME 48, 339–344.

Cundall, P.A., 1986. Distinct element methods of rock and soil structure. In: Brown, E.T. (Ed.), Numerical and analytical methods in engineering rock mechanics.

Cundall, P.A., 1988. Formulation of a three-dimensional distinct element model part I – A scheme to detect and represent contacts in a system composed of many polyhedral blocks. International Journal of Rock Mechanics and Mining Science and Geomechanics Abstracts 25, 107–117.

Cundall, P.A., Jenkins, J.T., Ishibashi, I., 1989. Evolution of elastic moduli in a deforming granular assembly, In: Biarez, J., Gourvès, R. (Eds.), Powders and Grains.

Cundall, P.A., Strack, O.D.L., 1979. A discrete numerical model for granular assemblies. Géotechnique 9, 47–65.

Digby, P.J., 1981. The effective moduli of porous granular rock. Journal of Applied Mechanics, Transactions of the ASME 48, 803–808.

Drescher, A., de Josselin de Jong, G., 1972. Photoelastic verification of a mechanical model for the flow of a granular material. Journal of the Mechanics and Physics of Solids 20, 337–351.

Horne, M.R., 1965. The behaviour of an assembly of rotound, rigid, cohesionless particles I and II. Proceedings of the Royal Society London A 286, 62–97.

de Josselin de Jong, G., Verruijt, A., 1969. Etude photo-elastique d'un empilement de disques. Cahier Groupe Francais Rheologie 2, 73–86.

Kruyt, N.P., Rothenburg, L., 1996. Micromechanical definition of the strain tensor for granular materials. Journal of Applied Mechanics, Transactions of the ASME 63, 706–711.

Kruyt, N.P., Rothenburg, L., 1998. Statistical theories for the elastic moduli of two-dimensional assemblies of granular materials. International Journal of Engineering Science 36, 1127–1142.

Liu, C.L., 1968. Introduction to combinatorial mathematics. McGraw-Hill, New York.

Oda, M., Konishi, J., 1974. Microscopic deformation mechanism of granular material in simple shear. Soils and Foundations 14, 25–38.

Oger, L., Savage, S.B., Corriveau, D., Sayed, M., 1998. Yield and deformation of an assembly of disks subjected to a deviatoric stress loading. Mechanics of Materials 27, 189–210.

Ostoja-Starzewski, M., Alzebdeh, K., Jasiuk, I., 1995. Linear elasticity of planar Delaunay networks III – Self-consistent approximations. Acta Mechanica 110, 57–72.

Prasher, C.L., 1987. Crushing and grinding process handbook. Wiley, Chichester, UK.

Rothenburg, L., 1980. Micromechanics of idealised granular materials. PhD Thesis Department of Civil Engineering, Carleton University, Ottawa, Ontario, Canada.

Rothenburg, L., Bathurst, R.J., 1991. Numerical simulation of idealised granular assemblies with plane elliptical particles. Computers and Geotechnics 11, 315–329.

Rothenburg, L., Bathurst, R.J., 1992. Micromechanical features of granular assemblies with planar particles. Géotechnique 42, 79–95.

Rothenburg, L., Selvadurai, A.P.S., 1981. A micromechanical definition of the Cauchy stress for particulate media. In: Selvadurai, A.P.S. (Ed.), Proceedings International Symposium on Mechanical Behaviour of Structured Media, Ottawa, Canada. pp. 469–486.

Satake, M., 1992. A discrete mechanical approach to granular materials. International Journal of Engineering Science 30, 1525–1533.

Strack, O.D.L., Cundall, P.A., 1978. The distinct element method as a tool for research in granular media: part I. Report National Science Foundation, NSF Grant ENG75-20711.

Ting, J.M., 1992. Robust algorithm for ellipse-based discrete element modelling of granular materials. Computers and Geotechnics 13, 175–186.

Tolman, R.C., 1938. The principles of statistical mechanics. Oxford University Press, Oxford, UK.

Walton, K., 1987. The effective elastic moduli of a random packing of spheres. Journal of the Mechanics and Physics of Solids 35, 213–226.